NRC Publications Archive
Archives des publications du CNRC

Calculation for the cathode surface concentrations in the electrochemical reduction of CO2 in KHCO3 solutions
Gupta, N.; Gattrell, M.; MacDougall, B.

© Springer 2005

Calculation for the cathode surface concentrations in the electrochemical reduction of CO_2 in $KHCO_3$ solutions

N. GUPTA, M. GATTRELL* and B. MACDOUGALL
National Research Council, Institute of Chemical Process and Environmental Technology, 1200 Montreal Road, Ottawa, ON, K1A 0R6, Canada
(*author for correspondence, Tel.: + 1-613-990-3819; e-mail: michael.gattrell@nrc-cnrc.gc.ca)

Abstract

This article presents a mathematical model that predicts the chemical conditions at the electrode surface during the electrochemical reduction of CO_2. Such electrochemical reduction of CO_2 to valuable products is an area of interest for the purpose of reducing green house gas emissions. In the reactions involved, CO_2 acts as both a reactant and a buffer, consequently the estimation of local concentrations at the electrode surface is not trivial and a numerical approach is required. The necessary partial differential equations (PDEs) have been set-up and solved using MATLAB. The results show the local concentrations at the electrode surface to be significantly different from the bulk concentrations under typical reported experimental conditions. The importance of buffer strength and a careful quantification of the degree of mixing produced in the experimental apparatus is demonstrated. The model has also been used to re-examine previously published data, showing that the Tafel slopes in CO_2 reduction are consistent with those reported for the simpler CO reduction system. Further, the effect of pulsed electroreduction was also modeled, showing that pulsing causes corresponding swings in local pH and CO_2 concentrations.

Nomenclature

Symbol	Description (Units)
cef_{CH_4}	current efficiency for methane formation (dimensionless)
$cef_{C_2H_4}$	Current efficiency for ethylene formation (dimensionless)
cef_{CO}	current efficiency for carbon monoxide formation (dimensionless)
cef_{H_2}	current efficiency for hydrogen formation (dimensionless)
cef_{HCOO^-}	current efficiency for formate formation (dimensionless)
$CO_{2\ consumption}$	rate of CO_2 consumption at cathode surface (kmol m^{-2} s^{-1})
$D^0_{CO_2}$	diffusion coefficient for carbon dioxide in water at 25 °C at infinite dilution (m^2 s^{-1})
$D^0_{CO_3^-}$	diffusion coefficient for carbonate ions in water at 25 °C at infinite dilution (m^2 s^{-1})
$D^0_{HCO_3^-}$	diffusion coefficient for bicarbonate ions in water at 25 °C at infinite dilution (m^2 s^{-1})
$D^0_{OH^-}$	diffusion coefficient for hydroxyl ions at 25 °C at infinite dilution (m^2 s^{-1})
D_{CO_2}	diffusion coefficient for carbon dioxide in water at 25 °C and given electrolyte concentration (m^2 s^{-1})
$D_{CO_3^-}$	diffusion coefficient for carbonate ions in water at 25 °C and given electrolyte concentration (m^2 s^{-1})
D_{HCO3^-}	diffusion coefficient for bicarbonate ions in water at 25 °C and given electrolyte concentration (m^2 s^{-1})
D_{OH^-}	diffusion coefficient for hydroxyl ions at 25 °C and given electrolyte concentration (m^2 s^{-1})
F	Faraday's constant (96486) (C mol^{-1})
j	current density at the Cu electrode (A m^{-2})
k_{1f}	rate constant for forward reaction (3b) (M^{-1} s^{-1})
k_{1r}	rate constant for reverse reaction (3b) (M^{-1} s^{-1})
k_{2f}	rate constant for forward reaction (4) (s^{-1})
k_{2r}	rate constant for reverse reaction (4) (s^{-1})

K_H	equilibrium constant for reaction (1) (dimensionless)
K_{1a}	equilibrium constant for reaction (3a) (M)
K_{1b}	equilibrium constant for reaction (3b) (M^{-1})
K_2	equilibrium constant for reaction (4) (M^{-1})
K_3	equilibrium constant for reaction (5) (dimensionless)
$OH^-_{formation}$	rate of OH^- formation at cathode surface (kmol m^{-2} s^{-1})
$zeff_{CH_4}$	electrons exchanged in reaction (13) (dimensionless)
$zeff_{C_2H_4}$	electrons exchanged in reaction (14) (dimensionless)
$zeff_{CO}$	electrons exchanged in reaction (12) (dimensionless)
$zeff_{H2}$	electrons exchanged in reaction (15) (dimensionless)
$zeff_{HCOO^-}$	electrons exchanged in reaction (11) (dimensionless)

Greek	**Description (Units)**
δ	boundary layer thickness (m)
μ	viscosity of electrolyte solution (mPa s or cP)

1. Introduction

With the steady rise in the demand for energy in the industrialized world, the use of fossil based fuels is also on the increase, causing an increase in the CO_2 emissions. The increased CO_2 emissions are a major concern as regards the green house effect. It is therefore of great interest to develop energy sources that do not rely on fossil fuels. While renewable energy can provide one solution, it is not always available at the time or location needed. Thus, methods to store such energy in a portable and easily used form are of interest. One approach is to collect CO_2 from air or power plant stacks, etc. and convert it back into fuels. This energy can then be used within existing infrastructures to displace fossil fuels, resulting in a net decrease of CO_2 emissions. This is especially important because it allows renewable energy to be applied to transportation applications, which represent a large and growing source of CO_2 emissions.

Electrochemistry represents an important enabling technology for this approach because of its high efficiency for conversion between electrical and chemical energy. Bandi et al. [1] have evaluated the energy demand for a process of CO_2 sequestration from air by absorption into KOH solutions followed by its conversion into fuel. CO_2 absorbed as potassium carbonate is separated by treating the solution with sulphuric acid and could then be electroreduced to useful fuels such as CH_4. The potassium sulphate solutions so produced by acidifying the potassium carbonate could be regenerated by electrodialysis.

Tryk and Fujishima [2] have shown the role electrochemists could play in reducing green house emissions by making fuels such as CO, CH_4 and C_2H_4 on various electrode materials such as Cu, Ni, Ag, etc. There is abundant literature on the electroreduction of CO_2 on various electrode materials [3]. The most recent review on CO_2 electroreduction has been done by Hori [4]. It has been reported by Teeter and Van Rysselberghe [5] and Ito et al. [6] that formate is exclusively produced in the cathodic reduction of CO_2 at metal electrodes (Hg, Au, Pb, Zn, Sn and In) in aqueous inorganic salt solutions. Further, work done by Steven et al. [7] has shown the reduction of CO_2 to CO with high current efficiency. Electrodes such as Ti, Ni, or Au have been studied for this application.

From a greenhouse gas reduction point of view, the most interesting reported results relate to the direct reduction of CO_2 to methane. At a copper electrode Hori et al. [8] reported that CO_2 can be directly electrochemically reduced to a mixture of hydrogen, methane, ethylene and CO.
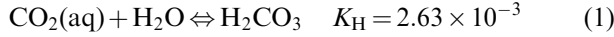
Studies done on CO_2 electroreduction use buffered (e.g. K_2HPO_4), somewhat buffered (viz. 0.1–0.5 M $KHCO_3$) and unbuffered (e.g. KCl, $KClO_4$, K_2SO_4) solutions with the majority using somewhat buffered solutions. In unbuffered solutions, the electrode local pH can vary widely from the bulk. In the somewhat buffered solutions, the equilibrium concentration of H_2CO_3 is very low and the kinetics of the reactions $CO_2(aq) + H_2O \Leftrightarrow H_2CO_3$ and $CO_2(aq) + OH^- \Leftrightarrow HCO_3^-$ are limited. This makes accurate estimation of the pH at the electrode surface an interesting problem. This is further complicated in this particular system by the fact that CO_2 is not only a part of the buffer, but is also the reactant. Thus the accurate estimation of the electrode surface conditions is not only additionally complicated, but is also doubly important for understanding what is happening in terms of the reaction mechanism.

Thus, the effect of pH at the electrode surface is important in mechanistic studies of CO_2 electroreduction. Hori et al. [9] pointed out this issue of the surface pH variation, and showed some simplified approximate calculations to illustrate the importance of the effects. However, in general, studies in the area fail to address the issue of electrode surface pH. Therefore, the intent of this work is to develop a detailed finite difference model to properly estimate the surface pH and CO_2 (reactant) concentration. The model will then be used to quantify the influence of variable current density and electrolyte
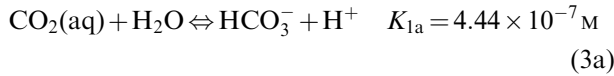
strength on the pH and to re-visit some results from the literature with a clearer insight.
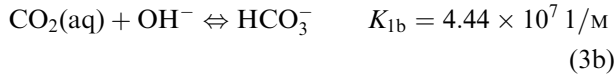
2. Theory

Various equilibrium reactions in the CO_2–$KHCO_3$ electrolyte system are (with the equilibrium constants at 25 °C from Sullivan et al. [3]):

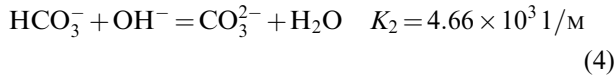$$CO_2(aq) + H_2O \Leftrightarrow H_2CO_3 \quad K_H = 2.63 \times 10^{-3} \quad (1)$$

$$H_2CO_3 \Leftrightarrow HCO_3^- + H^+ \quad (2)$$

Combining (1) and (2) gives:

$$CO_2(aq) + H_2O \Leftrightarrow HCO_3^- + H^+ \quad K_{1a} = 4.44 \times 10^{-7} \, \text{M} \quad (3a)$$

Or in basic solutions where pH > 7, Equation (3) is written as:

$$CO_2(aq) + OH^- \Leftrightarrow HCO_3^- \quad K_{1b} = 4.44 \times 10^7 \, 1/\text{M} \quad (3b)$$

Bicarbonate ion may be neutralized by OH^- ion generated on the cathode surface by:

$$HCO_3^- + OH^- = CO_3^{2-} + H_2O \quad K_2 = 4.66 \times 10^3 \, 1/\text{M} \quad (4)$$

Combining (3b) and (4) gives:

$$CO_2(aq) + CO_3^{2-} + H_2O \Leftrightarrow 2HCO_3^- \quad K_3 = 9.52 \times 10^3 \quad (5)$$
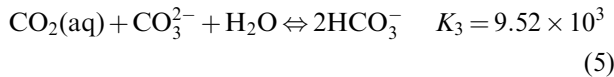
In the system under study, CO_2(gas) is in equilibrium with the liquid at all times, therefore CO_2(aq) concentration is a constant at a given pressure and temperature. So, for the electrolyte in equilibrium with CO_2 gas at a partial pressure of 101.3 kPa and a temperature of 25 °C, CO_2(aq) is 0.03416 M (i.e. ignoring the effect of ionic strength).

Initial concentrations (at time $t = 0$) of other species viz. HCO_3^-, CO_3^{2-} and pH may be determined by considering Equation (5) to be in equilibrium. While reaction (2) is fast, carbonic acid, H_2CO_3 never constitutes more than 1% of the total CO_2(aq) in solution, and so above a pH of 7.4, reaction (3b) dominates and reactions (1) and (2) can be ignored in the pH calculations [3].

Also, the kinetics of both the forward and reverse reactions of Equation (4) are very fast, so that it can be assumed that HCO_3^- is in equilibrium with CO_3^- at all times.

Figure 1 shows the electrode–electrolyte boundary layer in the CO_2 electroreduction system. Film theory is assumed to be applicable where, in the concentration boundary layer, the velocity gradients or convective effects are assumed to be negligible. The following balances would then occur within a slice of solution from x to $x + \Delta x$ in Figure 1:

$$\frac{\partial[CO_2(aq)]}{\partial t} = D_{CO_2}\frac{\partial^2[CO_2(aq)]}{\partial x^2} - [CO_2(aq)][OH^-]k_{1f} + [HCO_3^-]k_{1r} \quad (6)$$

$$\frac{\partial[HCO_3^-]}{\partial t} = D_{HCO_3^-}\frac{\partial^2[HCO_3^-]}{\partial x^2} + [CO_2(aq)][OH^-]k_{1f} - [HCO_3^-]k_{1r} - [HCO_3^-][OH^-]k_{2f} + [CO_3^{2-}]k_{2r} \quad (7)$$

$$\frac{\partial[CO_3^{2-}]}{\partial t} = D_{CO_3^-}\frac{\partial^2[CO_3^{2-}]}{\partial x^2} + [HCO_3^-][OH^-]k_{2f} - [CO_3^{2-}]k_{2r} \quad (8)$$

$$\frac{\partial[OH^-]}{\partial t} = D_{OH^-}\frac{\partial^2[OH^-]}{\partial x^2} - [CO_2(aq)][OH^-]k_f + [HCO_3^-]k_r - [HCO_3^-][OH^-]k_{2f} + [CO_3^{2-}]k_{2r} \quad (9)$$

The rate constants for the forward and reverse reactions (3b) and (4) are given in Table 1 and diffusion coefficients at infinite dilution in water for various species at 25 °C are listed in Table 2.
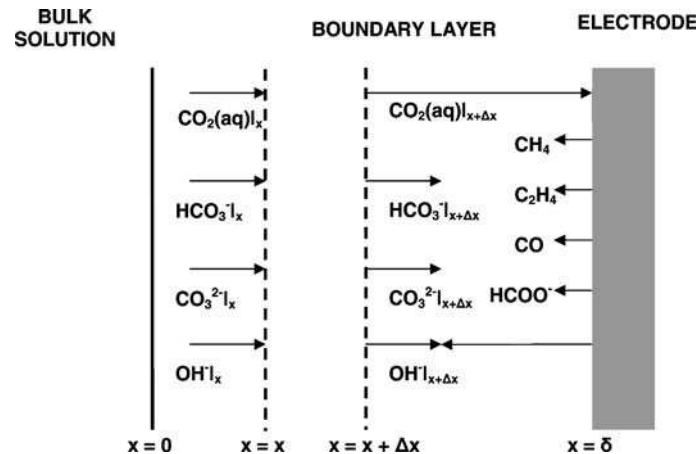

Fig. 1. Electrode–electrolyte boundary layer.

Table 1. Rate constants for reactions (3b) and (4) at 25 °C [3]

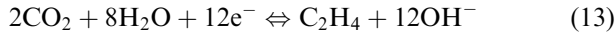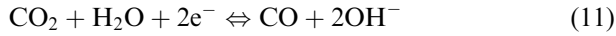| Reaction	Forward rate constant/$M^{-1}\ s^{-1}$	Reverse rate constant/s^{-1}
3b	$k_{1f} = 5.93 \times 10^3$	$k_{1r} = 1.34 \times 10^{-4}$
4	$k_{2f} = 1 \times 10^8$ (assumed)	$k_{2r} = k_{1f}/K_2 = 2.15 \times 10^4$

Table 2. Diffusion coefficients for CO_2, HCO_3^-, CO_3^{2-} at infinite dilution and OH^- at 25 °C in water [11]

$D^0_{CO_2}/m^2\ s^{-1}$	$D^0_{HCO_3^-}/m^2\ s^{-1}$	$D^0_{CO_3}/m^2\ s^{-1}$	$D^0_{OH^-}/m^2\ s^{-1}$
1.91×10^{-9}	9.23×10^{-10}	1.19×10^{-9}	5.27×10^{-9}

Table 3. Current efficiencies for different products in CO_2 electroreduction on Cu in 0.5 M $KHCO_3$ at 100 A m^{-2} and 25 °C [10]

Product	Electrons exchanged (zeff)	Current efficiency (cef)
CH_4	8	0.25
C_2H_4	12	0.20
CO	2	0.05
$HCOO^-$	2	0.10
H_2	2	0.40

CO_2 is reduced to a variety of products with different current efficiencies (see Table 3) according to overall reactions (10) to (13):

$$CO_2 + H_2O + 2e^- \Leftrightarrow HCOO^- + OH^- \qquad (10)$$

$$CO_2 + H_2O + 2e^- \Leftrightarrow CO + 2OH^- \qquad (11)$$

$$CO_2 + 6H_2O + 8\ e^- \Leftrightarrow CH_4 + 8OH^- \qquad (12)$$

$$2CO_2 + 8H_2O + 12e^- \Leftrightarrow C_2H_4 + 12OH^- \qquad (13)$$

Also water could be reduced to H_2 on Cu according to the following reaction

$$2H_2O + 2e^- \Leftrightarrow H_2 + 2OH^- \qquad (14)$$
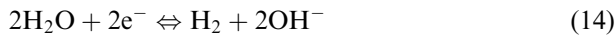
Table 3 lists the current efficiencies for different products obtained by the electroreduction of CO_2 on Cu. Based on these products, the current for CO_2 consumption and OH^- formation at the Cu electrode may be calculated as

$$CO_{2\,consumption} = \left(\frac{j}{F}\right)\left(\frac{cef_{HCOO^-}}{zeff_{HCOO^-}} + \frac{cef_{CO}}{zeff_{CO}} + \frac{cef_{CH_4}}{zeff_{CH_4}} + 2\left(\frac{cef_{C_2H_4}}{zeff_{C_2H_4}}\right)\right) \qquad (15)$$

$$OH^-_{formation} = \left(\frac{j}{F}\right)\left(\frac{cef_{HCOO^-}}{zeff_{HCOO^-}} + 2\left(\frac{cef_{CO}}{zeff_{CO}}\right) + 8\left(\frac{cef_{CH_4}}{zeff_{CH_4}}\right) + 12\left(\frac{cef_{C_2H_4}}{zeff_{C_2H_4}}\right)\right) \qquad (16)$$

where j is the planar current density on the electrode surface in A m^{-2}.

Equations (6)–(9) are second order time dependent partial differential equations which are to be solved under the following boundary conditions: The initial values of the concentrations (at $t = 0$, before current flows) are assumed to be the same in the bulk solution and are listed in Table 4 for different electrolyte concentrations. The diffusion coefficients in Table 2 were corrected for the viscosity change with varying electrolyte concentration (see Table 4) using Stokes–Einstein's equation ($D\mu/T$ = constant at $T = 298$ K) and these values of diffusion coefficients were used in Equations (6)–(9).

At time $t > 0$ and $x = 0$ (i.e. at the interface of bulk solution and the boundary layer):

$$CO_2(aq) = [CO_2(aq)]_i \qquad (17)$$

$$HCO_3^- = \left[HCO_3^-\right]_i \qquad (18)$$

$$CO_3^{2-} = \left[CO_3^{2-}\right]_i \qquad (19)$$

$$OH^- = [OH^-]_i \qquad (20)$$

where $[CO_2 (aq)]_i$, $[HCO_3^-]_i$, $[CO_3^{2-}]_i$, and $[OH^-]_i$ are the equilibrium values in the bulk solution, and so the same as the values given in Table 4. The boundary conditions at time $t > 0$ and $x = \delta$ (i.e. at the electrode surface) are related to the reaction fluxes.

$$D_{CO_2}\frac{d[CO_2(aq)]}{dx} = -CO_{2\,consumption} \qquad (21)$$

Table 4. Initial equilibrium values (at $t = 0$) for CO_2, HCO_3^-, CO_3^{2-}, OH^- and pH at different electrolyte ($KHCO_3$) concentrations at 25 °C and 101.3 kPa CO_2 partial pressure (Note: correction was not made for the effect of ionic strength on CO_2 solubility)

Electrolyte concentration/M	$CO_2(aq)$/M	HCO_3^-/M	CO_3^{2-}/ M	OH^-(M)	Ph	Viscosity (μ)/mPa s
0.05	0.0342	0.050	7.7×10^{-6}	3.3×10^{-8}	6.5	1.009
0.1	**0.0342**	**0.099**	3.1×10^{-5}	6.6×10^{-8}	**6.8**	**1.015**
0.2	0.0342	0.199	1.2×10^{-4}	1.3×10^{-7}	7.1	1.027
0.5	**0.0342**	**0.499**	7.6×10^{-4}	3.3×10^{-7}	**7.5**	**1.067**
1	0.0342	0.994	0.003	6.6×10^{-7}	7.8	1.145
2	0.0342	1.976	0.012	1.3×10^{-6}	8.1	1.319

$$D_{HCO_3^-} \frac{d[HCO_3^-]}{dx} = 0 \qquad (22)$$

$$D_{CO_3^-} \frac{d[CO_3^{2-}]}{dx} = 0 \qquad (23)$$

$$D_{OH^-} \frac{d[OH^-]}{dx} = OH_{formation}^- \qquad (24)$$

With all the boundary conditions and constants known, the partial differential equations given in (6)–(9) were solved using MATLAB 7.0.

3. Results and discussion

3.1. *General results*

Hori et al. [10] used Cu cathodes in 0.5 M KHCO₃ electrolyte for CO_2 electroreduction. For Hori's conditions, including the product distribution shown in Table 3, and based on their assumption of boundary layer thickness as 0.01 cm, the pH at the electrode surface may be calculated at different current densities by solving time-dependent partial differential equations (6)–(9).

For example, at a current density of 50 A m⁻² in 0.5 M KHCO₃ solution and a boundary layer thickness of 0.01 cm, the calculated pH and CO_2, HCO_3^- and

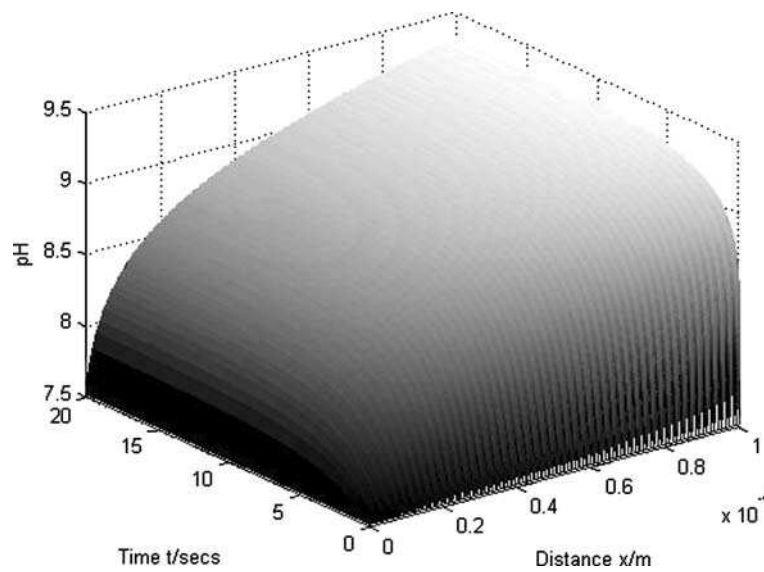*Fig. 2.* pH profile in the boundary layer at 50 A m⁻² (KHCO₃ = 0.5 M, δ = 0.01 cm).
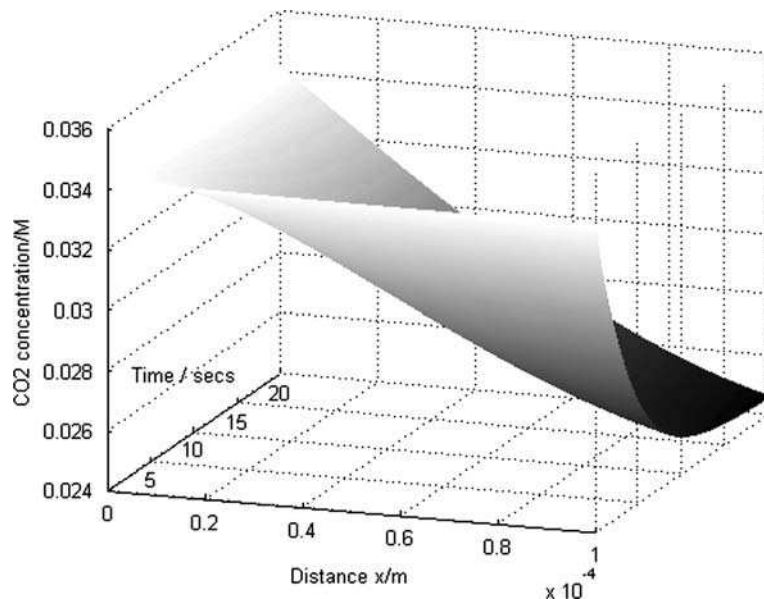
Fig. 3. CO_2 profile in the boundary layer at 50 A m⁻².

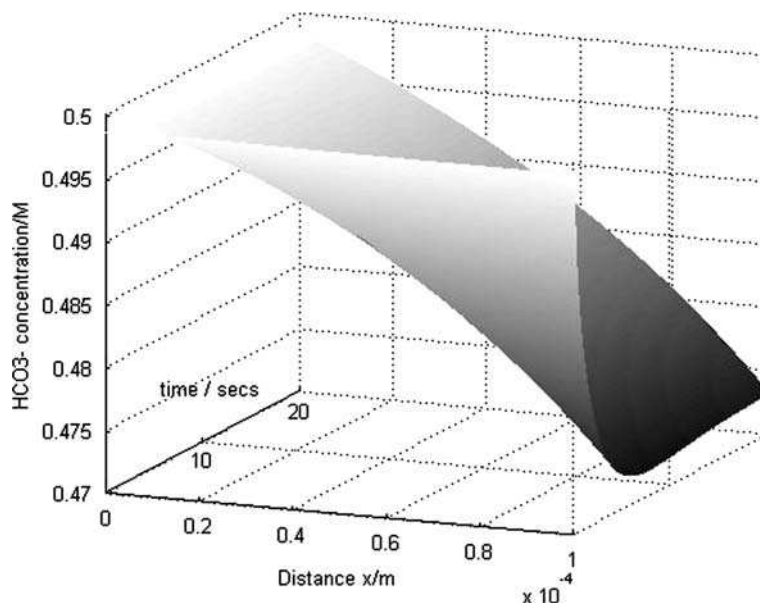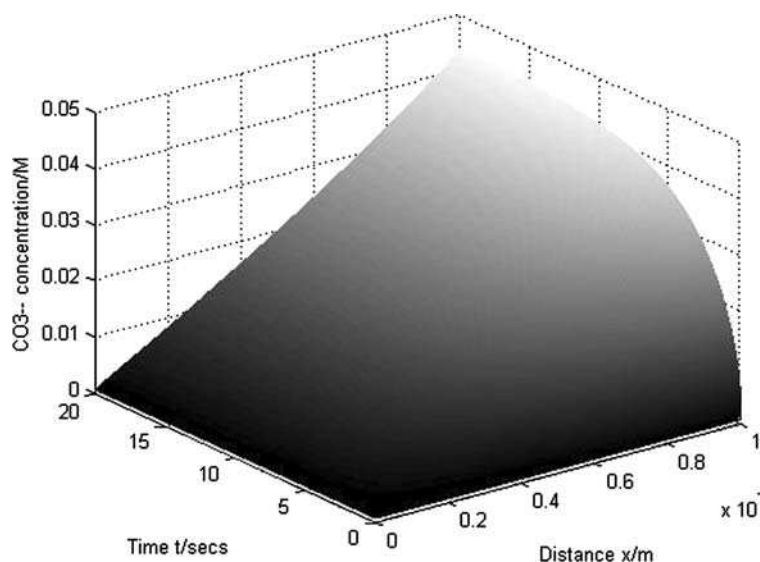*Fig. 4.* HCO_3^- profile in the boundary layer at 50 A m^{-2}.

Fig. 5. CO_3^{2-} profile in the boundary layer at 50 A m^{-2}.

CO_3^{2-} concentration profiles in the boundary layer may be observed in Figures 2–5, respectively. One can also see that the system takes roughly 10–12 s to reach steady state after the current is turned on (i.e. when the cathode is polarised). (Note that because pH is a logarithmic quantity, it appears to stabilise sooner). Before this period the concentrations of each of the species, i.e. CO_2, HCO_3^-, CO_3^{2-} and the pH at any given x (>0) in the boundary layer, is transient (varies with time).

Figure 2 further illustrates that the electrode surface pH at steady state ($t > 6$ s) is 9.3 which is considerably different from the bulk solution pH of 7.5. The reason for this increased pH is the generation of OH^- ions at the electrode surface. This increased surface pH may be critical to the mechanism of CO_2 electroreduction to various products viz. CH_4, C_2H_4, CO, $HCOO^-$ and H_2

as the product distribution might be expected to be affected by the relative amounts of CO_2 and H^+ present at the electrode surface (discussed later). The stabilization of the local pH at the electrode surface around pH 9.3 is due the actions of both CO_2 (reaction 3b, which produces bicarbonate) and the buffering action of bicarbonate (reaction 4, which consumes bicarbonate and produces carbonate). This buffer action within the boundary layer can be seen in Figures 3–5.

One can also see, in Figure 3, the non-linearity of the steady-state profile for the CO_2 concentration. This is due to CO_2 reacting at both the electrode surface, in electrochemical reactions, and in the boundary layer, in acid–base reactions. It is this complexity that creates the need for numerical calculation methods.
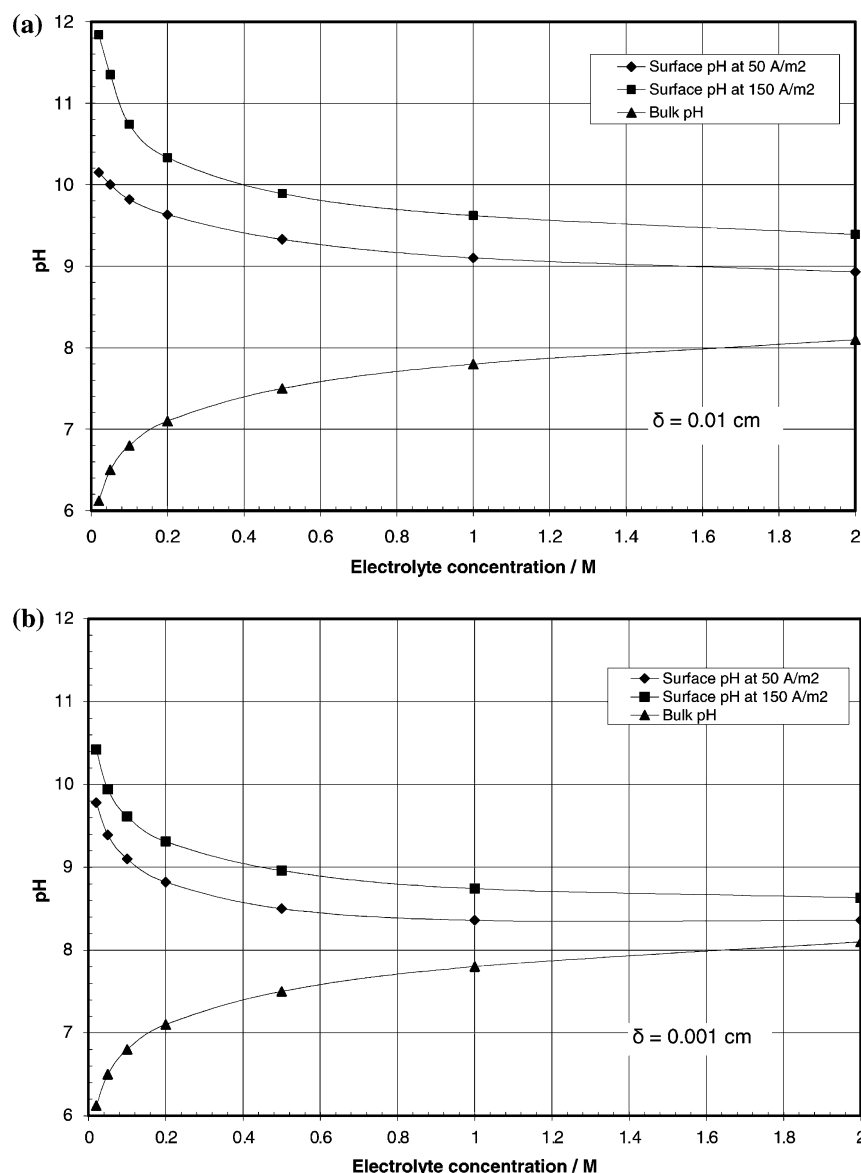
Fig. 6. Cathode surface pH vs. electrolyte concentration at δ = 0.01 and 0.001 cm.

Figure 6 shows the electrode surface pH profiles at 50 and 150 A m^{-2} and the bulk pH profiles as a function of the electrolyte concentration with boundary layer thicknesses (δ) of 0.01 and 0.001 cm. It is observed that the electrode surface pH at 50 and 150 A m^{-2} approaches the bulk pH value with increasing electrolyte strength. This pH approach occurs due to a rise in buffer capacity of electrolytes with increased concentrations. Specifically, this is due to a higher starting concentration of bicarbonate as can be seen in Table 4. On the other hand, the cathode surface pH may increase to 9.87 at 150 A m^{-2} from 9.3 at 50 A m^{-2} in a 0.5 M KHCO$_3$ solution with δ = 0.01 cm. This increase in pH occurs due to an increased generation rate of OH$^-$ on the cathode surface with increasing current density. This is obviously something that should be considered when comparing data measured at different current densities.

The profiles in Figure 6a are calculated for a boundary layer thickness of 0.01 cm (equivalent to an rpm of ∼75 at a rotating disc electrode), correspond to the estimated value of boundary layer thickness used by Hori et al. [9]. However, the boundary layer thickness depends on the stirring rate or the flow profile in a given electrochemical system (and/or the CO$_2$ bubbling rate). If the electrolyte is stirred at a higher rate or if the flow velocity is increased in a given flow cell, the boundary layer thickness will decrease and thereby alter the electrode surface pH (the effect on boundary layer due to viscosity variation with electrolyte concentration has been neglected in the present calculations).

Figure 6b illustrates a case where the boundary layer thickness has been decreased by an order of magnitude from that in Figure 6a (equivalent to increasing the rotation rate of an RDE by two orders of magnitude). With this thinner boundary layer, δ = 0.001 cm, it is

observed from Figure 6b that electrode surface pH approaches the bulk pH more closely than it does at $\delta = 0.01$ cm. Physically the closer approach may be explained by the fact that a better mixing of the electrolyte causes a more uniform solution pH. This is an important consideration because many papers studying the electrochemical reduction of CO_2 do not clearly define the degree of mixing used in their work, making the local pH and CO_2 concentrations at the electrode surface difficult to estimate. For example, for 0.5 M bicarbonate and 50 A m^{-2}, the local pH varies from 9.3 when $\delta = 0.01$ cm, to 8.5 when $\delta = 0.001$ cm.

3.2. Data analysis

To show the value of solving the equations and estimating the true conditions at the electrode surface, we have re-examined some data that has appeared in the literature. Hori et al. [9] have carried out experiments using a range of electrolyte strengths from 0.03 to 1.5 M, which resulted in different product distributions. In their paper, it is felt that the change in local pH values with the different buffer strengths plays a role in the obtained product distributions. We have used our model to more accurately estimate the exact pH and CO_2 concentrations, with the results of our calculations shown in

Figure 7 along with the current efficiency values from Hori's work.

In plotting these data, one can see a clear shift to less hydrogenated products with higher local pH. This effect dominates over the slight decrease that occurs in the local CO_2 concentration. On going from the 1.5 M buffer to the 0.03 M buffer, the local CO_2 concentration decreases by two times while the H$^+$ concentration decreases by about 15 times. This decrease in local CO_2 concentration is driven by a higher current efficiency for CO_2 consuming reactions and a higher rate of reaction 3b as the pH increases.

We also examined polarisation measurements made by Hori et al. [9]. The data has been re-plotted along with estimates for the local H$^+$ and CO_2 concentrations in Figure 8. Initially, the results show hydrogen evolution, which results in a local pH shifting from the bulk value of 6.81 to close to pH 9 by -1 V (10 A m^{-2}). At this potential, adsorbed CO begins to form, suppressing the hydrogen evolution, resulting in a slight decrease in current and an increase in local pH [13]. Below -1.12 V, hydrocarbon products begin to form, with first ethylene, then methane appearing. These reactions accelerate, causing a rapid rise in current at potentials below -1.26 V (8.5 A m^{-2}). Along with the increased reactions, there is a slight (about 2.1 times) decrease in local
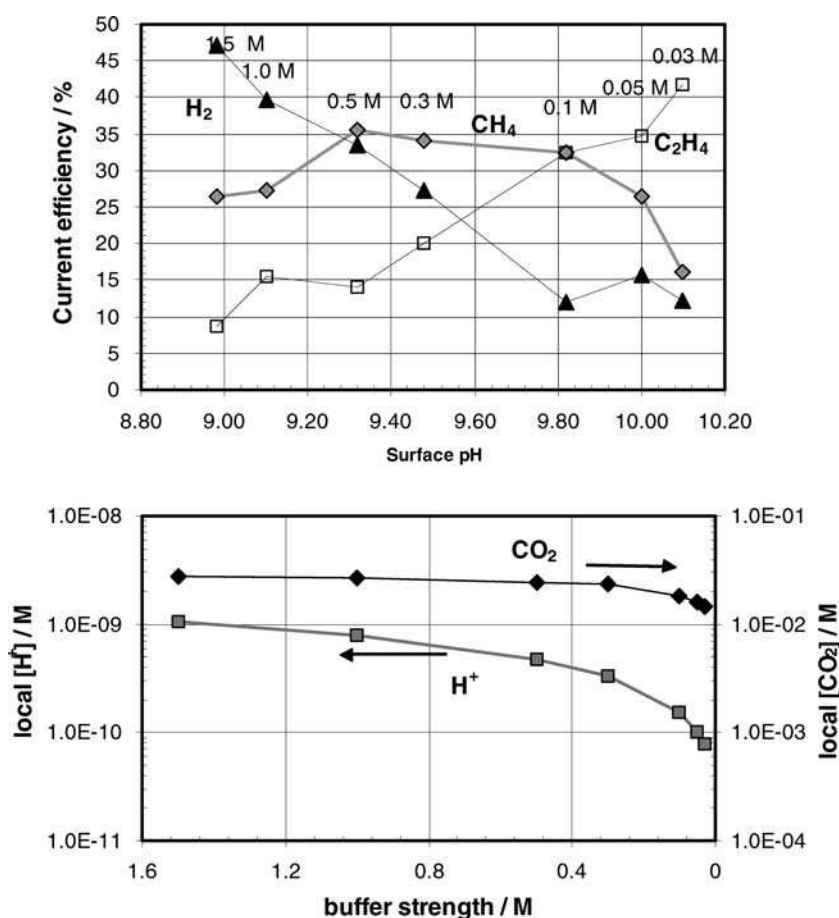

Fig. 7. The influence of buffer strength on the product distribution (Current efficiency data from Hori et al. [9], 50 A m^{-2}, potential -1.28 V vs. SHE at 1.5 M varying to -1.42 V at 0.03 M KHCO$_3$ buffer, CO_2 bubbled).
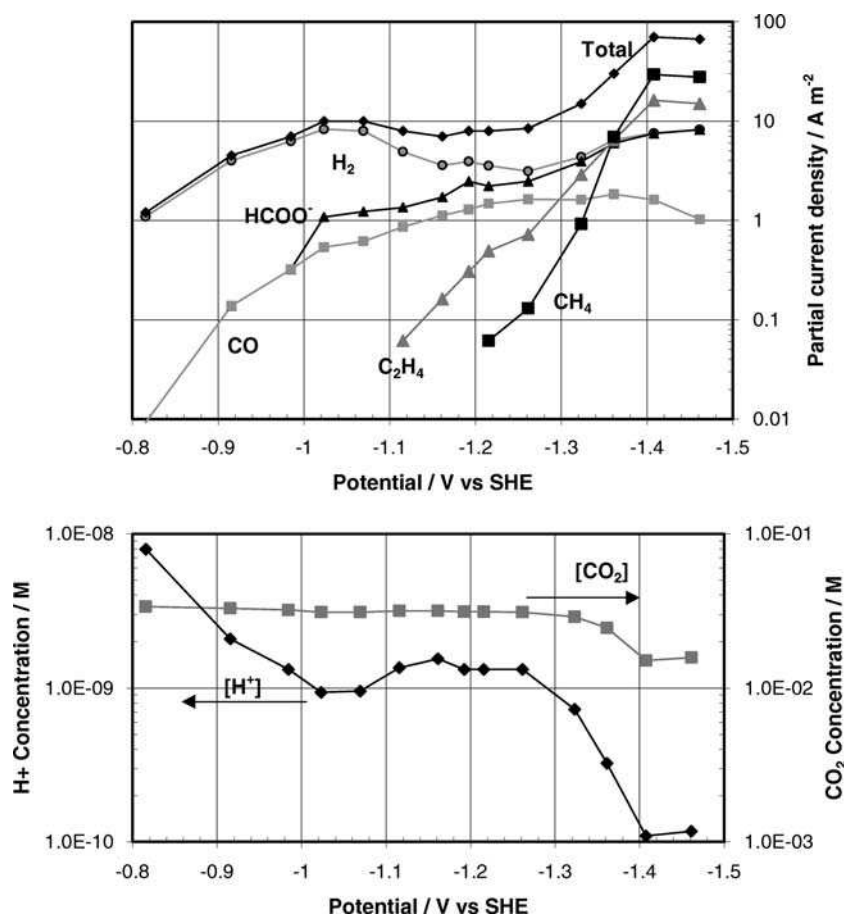
Fig. 8. Estimated local $[H^+]$ and $[CO_2]$ values for polarisation measurements (Partial current data from Hori et al. [9], 0.1 M KHCO$_3$, CO$_2$ bubbled, bulk $[H^+] = 1.55 \times 10^{-7}$ M, bulk $[CO_2] = 3.41 \times 10^{-2}$ M).

CO$_2$ concentration and a large decrease in local H^+ concentration (about a 12 times decrease leading to a local pH of 9.96 vs. 6.8 in the bulk solution).

It is interesting to note that, while high pH favoured ethylene in Figure 7, in this data set the increased potential seems to be able to overcome the effect. A key study on the influence of potential on these types of reactions was carried out by Hori et al. [12] using CO as the starting reactant. This system was studied because it is simpler, both in having fewer reaction steps and because CO is not involved in acid–base reactions, thus simplifying the estimation of the local CO concentration at the electrode surface. In that work, they found the reaction to form ethylene first order with respect to CO and having a charge transfer coefficient of 0.35 (171 mV decade^{-1} Tafel slope) and the reaction to form methane first order in CO, first order in hydrogen ion and having a charge transfer coefficient of 1.33 (45 mV decade^{-1} Tafel slope). From the data shown in Figure 8, one would obtain a charge transfer coefficient of 0.48 (124 mV decade^{-1} Tafel slope) for ethylene production and 0.86 (69 mV decade^{-1} Tafel slope) for methane production (obtained by excluding the data at −1.46 V). However, having the estimated local concentrations at the electrode surface should allow one to correct the data. For the methane data, assuming the reaction from CO$_2$ is also first order in hydrogen ion, we can correct the partial current densities by $[H^+]_{bulk}/[H^+]_{local}$. This results in a charge transfer coefficient of 1.19 (50 mV decade^{-1} Tafel slope), which is similar to that reported for methane for CO reduction, supporting the possibility of a similar mechanism. While we also have data for $[CO_2]_{local}$, correcting the partial currents would be complicated by the near saturation adsorption of the CO intermediate [13]. Because of the associated isotherm, this would be expected to lead to a non-linear relationship between $[CO_2]_{local}$ and the partial currents. However, knowing the local concentrations is also important and useful in any attempt to clarify the details of the reaction mechanisms.

3.3. *Pulsed CO$_2$ reduction*

A common problem reported associated with the electroreduction of CO$_2$ on Cu is the "poisoning" of the electrodes, which is characterised not by a significant change in total current (or potential), but by a shift in the product distribution over time to favour hydrogen evolution. Various theories have been put forward including electrolyte trace impurity deposition, accumulation of adsorbed or insoluble reaction by-products, and copper surface morphological changes [14]. However, the real cause for the poisoning is still not clear from the literature. In the recent review by
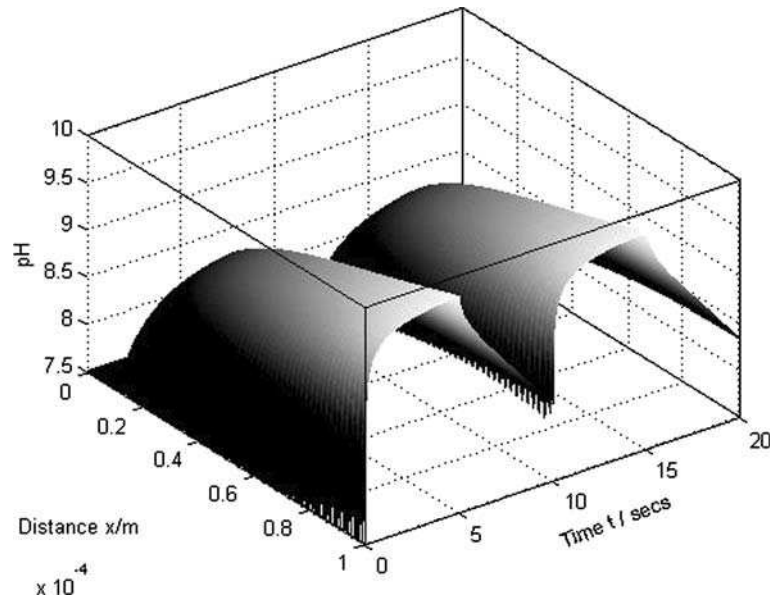
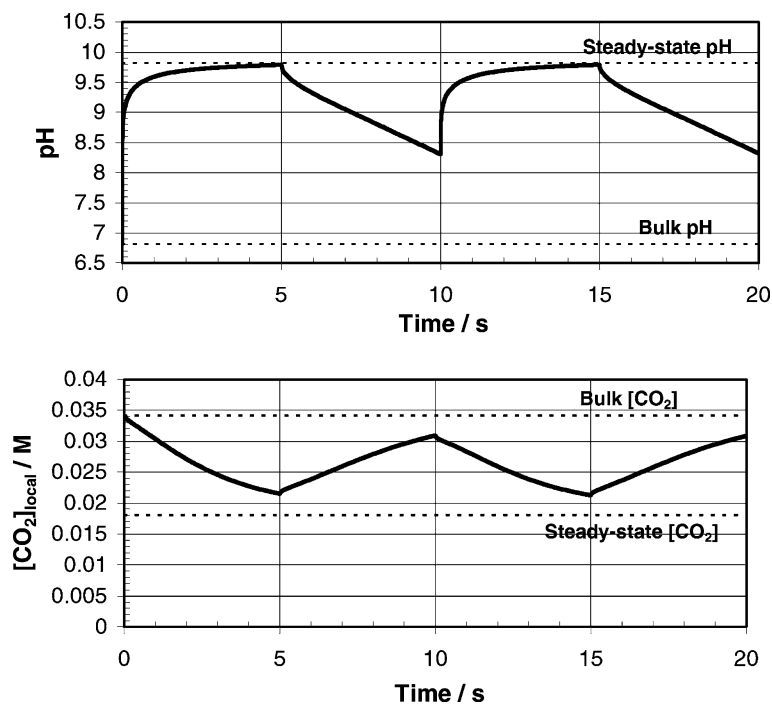*Fig. 9.* Pulsed pH profile in the boundary layer (50 A m^{-2}, 5 s then 0 A m^{-2}, 5 s, 0.1 M KHCO$_3$, δ = 0.01 cm).

Fig. 10. Pulsed surface pH and CO$_2$ profiles with bulk and steady state concentrations indicated (50 A m^{-2}, 5 s then 0 A m^{-2}, 5 s, 0.1 M KHCO$_3$, δ = 0.01 cm).

Hori et al. [4], the poisoning is attributed to the deposition of trace metal ions present in the KHCO$_3$ salts (ppm level) destroying the Cu catalytic activity. He recommends that the contaminants be removed using pre-electrolysis. However, Smith et al. [15] and others have claimed copper oxide type species to be the real cause of poisoning and according to them pre-electro-lyzing only postpones the inadvertent poisoning of the electrodes.

Even though the exact cause of poisoning is not clear, it has been found that poisoning of Cu electrodes may be avoided by pulsed potentials [16] or periodic anodic sweep treatments [17]. In the work of Shiratsuchi et al. [16], they tested pulsed waveforms stepping between −1.8 and 0 V vs. SCE, using a varying anodic pulse time from 0 to 10 s in an interval of 10 s. By pulsing the electrodes, the activity of Cu electrodes did not deteri-orate even after several hours of operation. Because of the complexity of the CO$_2$ solution chemistry, it should be noted that such a pulsing (or sweeping) regime will not only change the potential of the electrode, but also the local chemical conditions at the electrode surface.
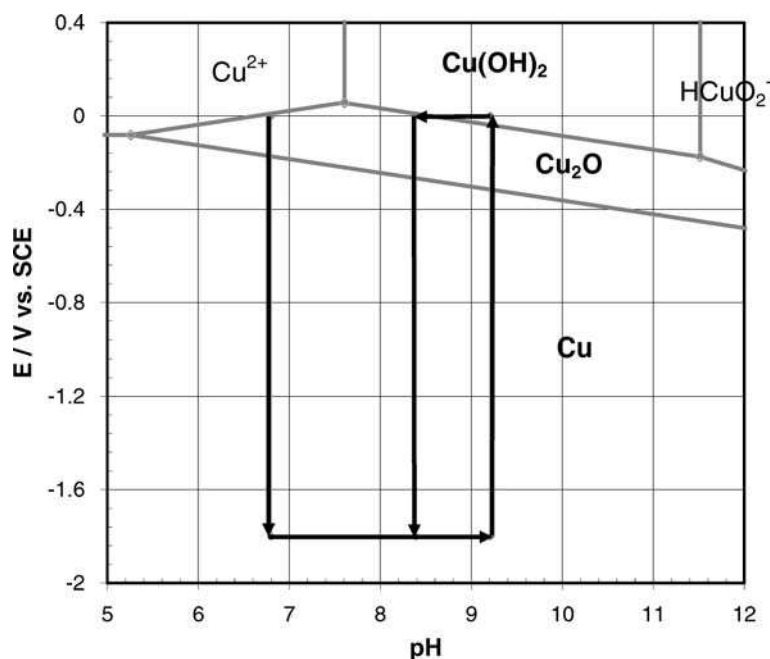
Fig. 11. A Pourbaix diagram for copper, indicating the regions traversed when the electrode is pulsed (50 A m^{-2}, 5 s then 0 A m^{-2}, 5 s, 0.1 M KHCO$_3$, δ = 0.01 cm) at 25 °C.

We have therefore also looked at estimating the local concentrations of CO$_2$ and hydrogen ion under pulsing conditions.

In the theoretical framework one needs to solve the differential equations (6)–(9) with changing boundary conditions. However, because the boundary conditions are written in terms of fluxes, it is simpler mathematically to assess the influence of pulsing using an equivalent galvanostatic pulse. Hence, the boundary conditions for CO$_2$ (Equation (21)) and OH$^-$ flux (Equation (24)) at the electrode surface were repeatedly changed from 50 A m^{-2} for 5 s to 0 A m^{-2} for 5 s (using the product distribution in Table 2). An electrolyte concentration of 0.1 M KHCO$_3$ (bulk pH = 6.8 cf. Table 4) was also used. These conditions roughly correspond to the best conditions reported in the work of Shiratsuchi et al. [16]. The changing pH profile so obtained is plotted in Figure 9, with the electrode surface hydrogen ion and CO$_2$ concentrations plotted in Figure 10.

The local CO$_2$ concentration is depleted during the cathodic pulses, but before the steady state concentration is achieved, the non-reducing part of the waveform allows fresh CO$_2$ to diffuse to the electrode. This results in an average local CO$_2$ concentration of 0.0263 vs. 0.0181 M for the steady state conditions (the 0.1 M case in Figure 7). One can also see that the predicted pH varies over a range of almost 1.5 pH units during the pulsing. In reality the pH variation could be higher because our model does not include the formation of copper oxides, which would consume local hydroxide ions. Also, the model uses a constant product distribution, which in reality would be changing with local concentrations and electrode potential. However, even this simplified model shows changes in local conditions, which should be considered when investigating the mechanism for the electrode regeneration.

In Figure 11, a Pourbaix diagram for Cu is shown with the system's state over the course of the electrode pulsing indicated. The system starts at 0 V (taken to be 0 current) then is shifted to −1.8 V (taken to be a current of 50 A m^{-2}). As the electrode is held at −1.8 V the local pH increases from the bulk value of 6.82 to 9.79. On returning to 0 V, the pH tends back towards the bulk value, reaching 8.31 after 5 s. It can be seen that, over the latter pH drift, the stable form of copper oxide would change from Cu(OH)$_2$ to Cu$_2$O. This underlines the importance of considering the local chemical conditions at the electrode surface in understanding these complex reactions.

4. Conclusions

A model has been developed for calculating the electrode surface hydrogen ion and CO$_2$ concentrations for CO$_2$ electroreduction on Cu in KHCO$_3$ electrolyte solution. The modelled results show that the electrode surface conditions are dependent on the stirring rate, buffer capacity of the electrolyte and the current density of operation. It has also been shown using the model estimates that the stirring rate results in a significant change in the local concentrations (cf. Figure 6). This is important because results from other workers have shown that the CO$_2$ reduction product distribution is affected by hydrogen ion concentration, potential (current density), and CO$_2$ concentration. Thus work in this area should try to quantify the level of stirring used. These results also depend strongly on the buffer capacity (electrolyte strength) used.

172

The developed model was also useful for correcting previously reported literature data, to show that the Tafel slopes observed for the production of methane and ethylene from CO_2 are similar to those reported for the formation of the same products from CO. Through adjustment of the boundary conditions, the model can be extended to roughly evaluate the response of local hydrogen ion and CO_2 concentrations to pulsed CO_2 reduction. This approach might prove useful in better understanding the role of pulsed operation in preventing electrode activity losses.

Thus, the model developed in this work should prove useful in furthering the understanding of the reactions involved in the electroreduction of CO_2 from carbonate buffers. In particular, it should be helpful in future mechanistic studies.

References

1. A. Bandi, M. Specht, T. Weimer and K. Schaber, *Energy Conv. Manag.* **36** (1995) 899.
2. D.A. Tryk and A. Fujishima, *Electrochem. Soc. Int.* **10** (2001) 32.
3. B.P. Sullivan, K. Krist and H.E. Guard (Ed., *Electrochemical and Electrocatalytic Reactions of Carbon Dioxide* (Elsevier, Amsterdam, 1993).
4. Y. Hori, in W. Vielstich and H.A. Gasteiger and A. Lamm (Eds), Handbook of Fuel Cells', (John Wiley and Sons, Ltd., West Sussex, England **2** 2003) p. 720.
5. T.E. Teeter and P. Van Rysselberghe, *J. Chem. Phys.* **22** (1954) 759.
6. K. Ito, T. Murata and S. Ikeda, *Bull. Nagoya Inst. Tech.* **27** (1975) 209.
7. G.B. Stevens, T. Reda and B. Raguse, *J. Electroanal. Chem.* **526** (2002) 125.
8. Y. Hori, K. Kikuchi and S. Suzuki, *Chem. Lett.* (1985) 1695.
9. Y. Hori, M. Akira and R. Takahashi, *J. Chem. Soc. Faraday Trans.* **1**(85) (1989) 2309.
10. Y. Hori, K. Kikuchi, A. Murata and S. Suzuki, *Chem. Lett.* (1986) 897.
11. D.R. Lide, *CRC Handbook of Chemistry and Physics, Internet Version 2005*, < http://www.hbcpnetbase.com >, (CRC Press, Boca Raton, FL, 2005).
12. Y. Hori, R. Takahashi, Y. Yoshinami and A. Murata, *J. Phys. Chem. B* **101** (1997) 7075.
13. Y. Hori, M. Akira and Y. Yoshinami, *J. Chem. Soc. Faraday Trans.* **1**(87) (1991) 125.
14. R.L. Cook, R.C. MacDuff and A.F. Sammells, *J. Electrochem. Soc.* **135** (1988) 1320.
15. B.D. Smith, D.E. Irish, P. Kedzierzawski and J. Augustynski, *J. Electrochem. Soc.* **144** (1997) 4288.
16. R. Shiratsuchi, Y. Aikoh and G. Nogami, *J. Electrochem. Soc.* **140** (1993) 3479.
17. B. Jermann and J. Augustynski, *Electrochim. Acta* **39** (1994) 1891.